

PAPER

Determination Method of Cascaded Number for Lumped Parameter Models Oriented to Transmission Lines

Risheng QIN^{†a)}, Hua KUANG^{††}, He JIANG[†], Hui YU[†], Hong LI^{†††}, and Zhuan LI^{††††}, *Nonmembers*

SUMMARY This paper proposes a determination method of the cascaded number for lumped parameter models (LPMs) of the transmission lines. The LPM is used to simulate long-distance transmission lines, and the cascaded number significantly impacts the simulation results. Currently, there is a lack of a system-level determination method of the cascaded number for LPMs. Based on the theoretical analysis and eigenvalue decomposition of network matrix, this paper discusses the error in resonance characteristics between distributed parameter model and LPMs. Moreover, it is deduced that optimal cascaded numbers of the cascaded π -type and T-type LPMs are the same, and the Γ -type LPM has a lowest analog accuracy. The principle that the maximum simulation frequency is less than the first resonance frequency of each segment is presented. According to the principle, optimal cascaded numbers of cascaded π -type, T-type, and Γ -type LPMs are obtained. The effectiveness of the proposed determination method is verified by simulation.

key words: distributed parameter model, lumped parameter model, resonance mode analysis, cascaded number, characteristic impedance

1. Introduction

Physical simulation technology is often used to investigate steady-state characteristic and transient-state characteristics of transmission lines [1]–[4]. Even though real-time digital simulation technology is widely used [5], physical simulation technology still holds an important position because it can intuitively reflect changes in electricity, especially under high voltage conditions. Generally, π -type and T-type circuits, or occasionally Γ -type circuits are applied to physically simulate the transmission line [6]–[9]. These three lumped parameter models (LPMs) have high analog accuracy in systems with low frequency and short lines. Due to the low operating frequency and short transmission distance, the wavelength of the voltage is so small that it can be ignored. For the network with high frequency and long lines [10], [11], such as high voltage direct current and half-wavelength AC transmission, the wavelength of the voltage accounts for a large proportion of the length of the transmission line [12]–[14]. Equivalent LPMs of these systems have

significant errors. In these systems, transmission lines have been integrated with series impedance and parallel admittance, which is known as distributed parameter effect [15]–[19].

Line resonance is caused by the interaction of parasitic impedance and capacitance to ground [20], [21]. Distributed parameter effect leads to inconsistent resonance characteristics between the line and the equivalent line. Therefore, the resonance characteristics of the LPMs also characterize the simulation accuracy. The distributed parameter model (DPM) has been proven to have periodic parallel and series resonance frequencies [22]. However, there is still a lack of system-level research on the impedance of multi-cascade transmission lines.

To accurately simulate the impedance and transmission characteristics of long lines, multiple-cascade short lines are often used to equivalent long lines [23]. The cascaded number not only affects the simulation accuracy but also affects the experimental cost. Too large cascades have high accuracy but also high cost. Reference [24] provided a simple method for determining the cascaded number. When the line length is less than one-thirtieth of the wavelength of the simulated highest frequency, the distributed parameter effect of the line can be ignored. In this case, π -type and T-type LPMs can be used to simulate frequencies below the highest frequency. However, this is still a considerable number. For example, for the 750 kV/500 km lossless line in [16], 155 segment LPMs are required to simulate the transmission characteristics of 3000 Hz. Reference [25] proposed a method for determining the cascaded numbers of cascaded π -type and T-type LPMs of lossless lines based on mathematical analysis. References [26], [27] discussed the difference in transient-state characteristics between DPM and LPM, and further determine the cascaded number through simulation. But the implementation is complex.

This paper discusses the difference in the resonance characteristics between DPM and LPMs of transmission lines. A method for determining the cascaded number for different cascaded LPMs is further presented. Based on resonance mode analysis (RMA) and theoretical analysis, the periodic resonance characteristics of DPM in open and short circuits are studied. The resonance differences between DPM and LPMs are discussed. The characteristic impedance of cascaded π -type and T-type LPM is derived from the single-segment LPM. The consistency of first resonance frequencies indicates that cascaded π -type and T-type LPMs have the same accuracy. The method for determining

Manuscript received September 1, 2023.

Manuscript revised November 1, 2023.

Manuscript publicized December 20, 2023.

[†]The authors are with Electric Power Research Institute, Yunnan Power Grid Co. Ltd., 650000, Kunming, China.

^{††}The author is with Yunnan Power Grid Co. Ltd., 650000, Kunming, China.

^{†††}The author is with Honghe Power Supply Bureau, Yunnan Power Grid Co. Ltd., 651400, Honghe, China.

^{††††}The author is with Dali Power Supply Bureau, Yunnan Power Grid Co. Ltd., 671000, Dali, China.

a) E-mail: qinrisheng2020@126.com

DOI: 10.1587/transele.2023ECP5038

cascaded number based on the first resonance frequency of the single segment shows that the cascaded Γ -type LPM has low accuracy. Finally, the proposed determination method for LPMs is verified by simulation.

2. Resonance Characteristics of Transmission Lines

2.1 Resonance Mode Analysis Method

Harmonic resonance means a drastic energy exchange process in the network. The RMA technique can find the impedance elements with violent energy exchange in the resonance network [28], [29]. It is based on the eigenvalue decomposition of the admittance matrix and the implementation is expressed as follows:

$$\mathbf{V}_f = \mathbf{Y}_f^{-1} \mathbf{I}_f \quad (1)$$

where \mathbf{V}_f is the node voltage matrix. \mathbf{Y}_f is the node admittance matrix. \mathbf{I}_f is the nodal current injection matrix. The eigenvalue decomposition of \mathbf{Y}_f is expressed as

$$\mathbf{Y}_f = \mathbf{L} \mathbf{A} \mathbf{T} \quad (2)$$

where \mathbf{L} and \mathbf{T} are the left eigenvector matrix and right eigenvector matrix, respectively. \mathbf{A} is the diagonal eigenvalue matrix. Substituting (2) into (1) yields

$$\mathbf{V}_f = \mathbf{L} \mathbf{A}^{-1} \mathbf{Y}_f^{-1} \mathbf{L}^{-1} \mathbf{I} \quad (3)$$

$\mathbf{U}_f = \mathbf{L}^{-1} \mathbf{V}$ and $\mathbf{J}_f = \mathbf{L}^{-1} \mathbf{I}$ are defined as modal voltage vector and modal current vector, respectively. Equation (3) can be expressed as

$$\begin{bmatrix} U_{f1} \\ U_{f2} \\ \vdots \\ U_{fn} \end{bmatrix} = \begin{bmatrix} \lambda_{f1}^{-1} & 0 & 0 & 0 \\ 0 & \lambda_{f2}^{-1} & 0 & 0 \\ & 0 & \ddots & 0 \\ 0 & 0 & 0 & \lambda_{fn}^{-1} \end{bmatrix} \begin{bmatrix} J_{f1} \\ J_{f2} \\ \vdots \\ J_{fn} \end{bmatrix} \quad (4)$$

The reciprocal of the λ_{fi} is resistive. The modal eigenvalues of resonance can be determined according to the eigenvalues. Therefore, RMA can quickly locate the resonance frequency and harmonic center.

2.2 Resonance Characteristics of DPM

When the signal transmitted on the line is at power frequency, the length is much smaller than the signal wavelength, and the line is considered a short line. When the transmitted signal is in the high-frequency range, the length is in the same order of magnitude as the signal wavelength. The analysis cannot be based on the circuit theory at low frequencies. The resonance characteristics should be analyzed using the equivalent circuit with distributed resistance, capacitance, and inductance. Figure 1 shows the distributed parameter model of the line. In the figure, R_0 , L_0 , G_0 ($= 0$), C_0 are the inductance, resistance, conductivity, and susceptance of unit length. The parameters of the DPM are shown in Table 1.

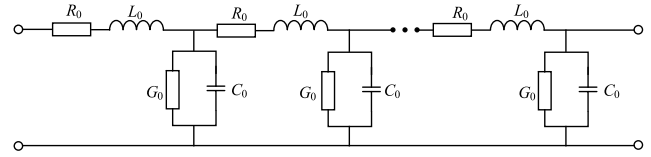


Fig. 1 The DPM of the transmission line.

Table 1 Transmission line parameters.

Parameter Description	Symbol	Value
Fundamental frequency	f_0	50 Hz
Electrical parameters per unit length	R_0	0.08 Ω /km
	L_0	0.95 mH/km
	C_0	0.47 μ F/km
Attenuation coefficient	α	0.0009
Phase coefficient	β	0.067
Characteristic impedance	Z_c	(45.3537-j5.973) Ω
Equivalent series impedance	Z_s	(2.393+j8.9) Ω
Equivalent parallel admittance	Y_p	j0.0045 S
Line length	l	30 km

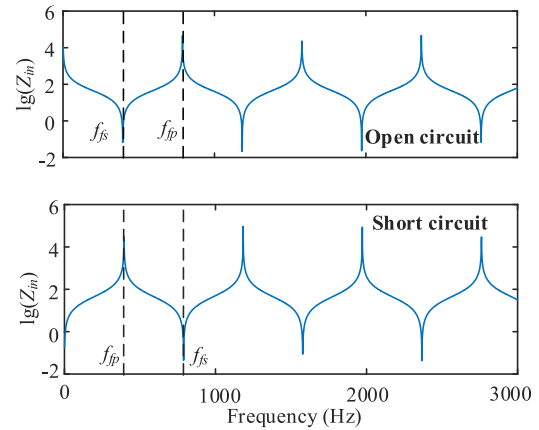


Fig. 2 The impedance characteristics of the input impedance.

According to transmission line theory, the input impedance Z_{in} of the line is

$$Z_{in} = Z_c \frac{Z_l + Z_c \tanh(\gamma l)}{Z_l \tanh(\gamma l) + Z_c} \quad (5)$$

where Z_l is the load impedance at the end of the line. Z_c , and γ are characteristic impedance, and line propagation coefficient. They are expressed as

$$\begin{cases} Z_c = \sqrt{(R_0 + j\omega L_0)/j\omega C_0} \\ \gamma = \sqrt{j\omega C_0(R_0 + j\omega L_0)} \end{cases} \quad (6)$$

When the transmission line is open, Z_{in} is

$$Z_{in} = -jZ_c \cot(\omega l \sqrt{L_0 C_0}) \quad (7)$$

The amplitude-frequency characteristics of Z_{in} is shown in Fig. 2. Figure 2 shows that the input impedance alternately exhibits inductance and capacitance as the frequency increases. The series resonance frequency and parallel resonance frequency are periodic, and the periods are the same. According to (7), the first series and parallel resonance frequencies are

$$f_{fs} = 1/(4l\sqrt{L_0C_0}) = 395 \text{ Hz}, \quad f_{fp} = 2f_{fs} \quad (8)$$

When the line end is shorted, the input impedance Z_{in} of the transmission line is

$$Z_{in} = Z_c \coth(\gamma l) = jZ_c \tan(\omega l \sqrt{L_0C_0}) \quad (9)$$

The amplitude-frequency characteristics of input impedance is shown in Fig. 2. It can be seen that the input impedance also alternately presents inductance and capacitance. Similarly, it can be obtained that the first series and parallel resonance frequencies are 789 Hz and 395 Hz, respectively.

When the transmission line is open circuit and shorted circuit, the modal information is shown in Fig. 3. The resonance characteristics of the lines can be more directly understood through RMA. Figure 3 indicates that the parallel resonance frequency of the open circuit is equal to the series resonance frequency of the short circuit. Similarly, the series resonance frequency of the open circuit is equal to the parallel resonance frequency of the short circuit. This can also be verified by (8).

In addition, modern transmission harmonics have the characteristics of high frequency and wide frequency domain, so the high-frequency skin effect (HFSE) of lines must be considered [30], [31]. With the HFSE, parasitic resistance increases with the harmonic frequency. The unit equivalent resistance r is

$$r = \frac{R_0}{1 - (1 - \sqrt{j2\pi f_0/s})^2} \quad (10)$$

The resonance frequency and modal impedance of the transmission line are shown in Table 2. As can be seen, HFSE only plays a role in suppressing resonance peak. When the cascaded number is determined only by the resonance frequency, the HFSE will not affect the results.

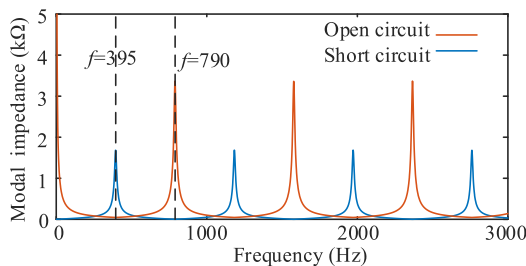


Fig. 3 The modal impedance of the input impedance.

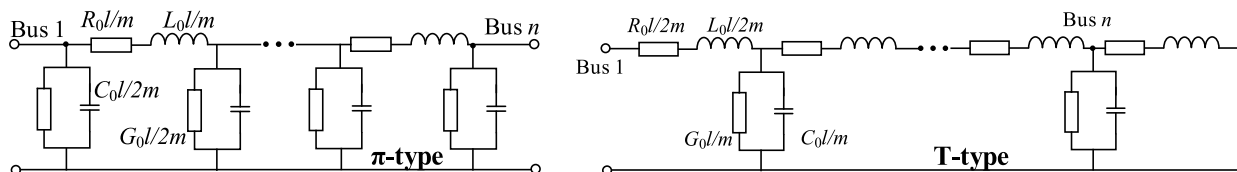


Fig. 4 The topology of cascaded LPM.

2.3 Resonance Characteristics of Cascaded π -Type LPM

When the end of the cascaded π -type LPM is shorted, the terminal capacitor will be shorted. Therefore, this paper discusses the resonance characteristic of the π -type LPM when the end is open. The π -type LPM with cascaded number m is shown in Fig. 4 (a). The corresponding admittance matrix $Y_{\pi-m}$ is

$$Y_{\pi-m} = \begin{bmatrix} Y_{11} & Y_{12} & \cdots & 0 \\ Y_{21} & Y_{22} & \cdots & 0 \\ \vdots & \vdots & \ddots & \vdots \\ 0 & 0 & \cdots & Y_{mm} \end{bmatrix} \quad (11)$$

The non-zero elements in the matrix are

$$Y_{ij} = \begin{cases} -m/(R_0l + j\omega L_0l) & i = j \pm 1 \\ (G_0 + j\omega C_0)l/m + 2m/(R_0l + j\omega L_0l) & i = j = (2, \dots, n-1) \\ (G_0 + j\omega C_0)l/2m + m/(R_0l + j\omega L_0l) & i = j = 1, n \end{cases} \quad (12)$$

The modal information of the π -type LPM with different cascaded numbers is shown in Fig. 5. Figure 5 shows that the number of the parallel resonance frequency is the same as the cascaded number. The first resonance frequency increases with the cascaded number and gradually closes to f_{fp} . In other words, the accuracy of the cascaded π -type LPM increases with the cascaded number. This is consistent with empirical facts.

The input impedance $Z_{in,\pi}$ of a single segment is:

Table 2 Modal information of the transmission line.

	Without HFSE		With HFSE	
	Resonance frequency (Hz)	Modal peak (Ω)	Resonance frequency(Hz)	Modal peak (Ω)
open	395	1683.6	395	988.1
	1183	1684.7	1183	622.7
	1972	1684.4	1972	495
	2761	1681.9	2761	422.5
shorted	789	3366.4	789	1476.9
	1578	3359	1578	1089.7
	2367	3347.2	2367	902.5
	3155	3369	3155	793

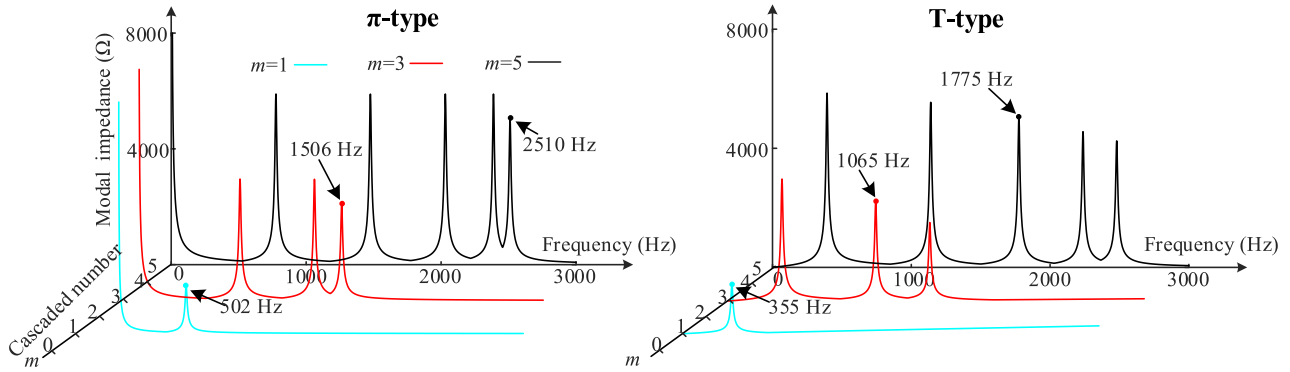


Fig. 5 Modal information of the cascaded LPM.

$$Z_{in_{\pi}} = \frac{1 - \omega^2 \left(\frac{l}{m} L_0 \right) \left(\frac{l}{2m} C_0 \right)}{j\omega \frac{l}{2m} C_0 \left(2 - \omega^2 \left(\frac{l}{m} L_0 \right) \left(\frac{l}{2m} C_0 \right) \right)} \quad (13)$$

When the denominator in (13) is zero, the input impedance of each segment is the largest. The frequency at this point is one of the parallel resonance frequencies, and this frequency is

$$f_{\pi_{-P}} = \frac{m}{\pi l \sqrt{L_0 C_0}} \quad (14)$$

When m is 1, 3, and 5, the $f_{\pi_{-P}}$ are 502 Hz, 1506 Hz, and 2510 Hz, respectively. This can be clearly seen from the modal information diagram. Notably, the modal information diagram indicates that these frequencies are also the last resonance frequencies of the cascaded π -type LPM.

2.4 Resonance Characteristics of Cascaded T-Type LPM

When the end of the cascaded T-type LPM is open, the terminal impedance will be open-circuited. Therefore, this paper discusses the resonance characteristics of the T-type equivalent circuit when the end is shorted. The cascaded T-type LPM of the line with cascaded number m is shown in Fig. 4. The modal information of the cascaded T-type LPM with different cascaded numbers is shown in Fig. 5. Figure 5(b) shows that the number of parallel resonance frequencies is the same as the cascaded number. As the cascaded number increases, the first resonance frequency of cascaded T-type LPM gradually approaches that of DPM. Therefore, the optimal cascaded number can be determined based on the first resonance frequency. This is consistent with the cascaded π -type LPM.

The input impedance $Z_{in_{\Gamma}}$ of a single segment is:

$$Z_{in_{\Gamma}} = \frac{j\omega \frac{l}{2m} L_0 \left(2 - \omega^2 \left(\frac{l}{2m} L_0 \right) \left(\frac{l}{m} C_0 \right) \right)}{\left(1 - \omega^2 \left(\frac{l}{2m} L_0 \right) \left(\frac{l}{m} C_0 \right) \right)} \quad (15)$$

The parallel resonance frequency is

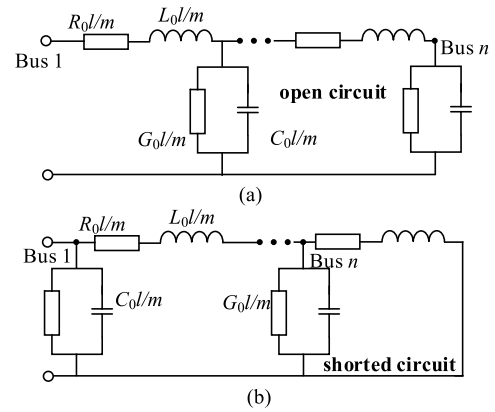


Fig. 6 The topology of cascaded Γ -type LPM.

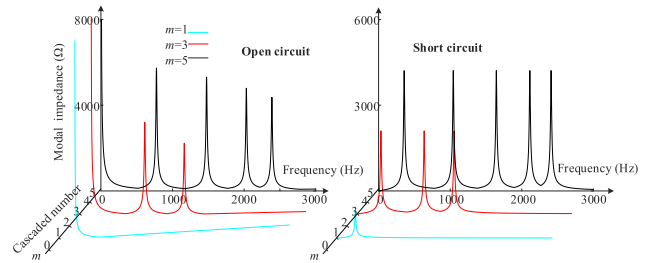


Fig. 7 Modal information of the Γ -type LPMs.

$$f_{\Gamma_{-P}} = \frac{\sqrt{2}m}{2\pi l \sqrt{L_0 C_0}} \quad (16)$$

When m is 1, 3, and 5, the $f_{\Gamma_{-P}}$ calculated by (16) are 355 Hz, 1065 Hz, and 1775 Hz, respectively. Compared with Fig. 5, these resonance frequencies are not the final resonance frequencies but appear in the middle. This is different from the cascaded π -type LPM.

2.5 Resonance Characteristics of Cascaded Γ -type LPM

When the line is open circuit and short circuit, the cascaded Γ -type models of the line with cascaded number m are shown in Fig. 6. The modal information of the Γ -type LPMs with different cascaded numbers is shown in Fig. 7. As can be seen, although both Γ -type models have $2m$ energy stor-

age elements, they have different resonance characteristics. Firstly, they have opposite phase frequency characteristics. In the low-frequency band, open circuit and shorted circuit are capacitive and inductive, respectively. Secondly, they have different resonance frequency quantities. The number of resonance frequencies in the open circuit is equal to the cascaded number minus 1. The number of resonance frequencies in the shorted circuit is equal to the cascaded number. Compared with Fig. 5 (b), it can be seen that when the line is shorted, the resonance frequency of each cascaded number is smaller than the resonance frequency of the cascaded T-type LPM. This indicates that the analog accuracy of cascaded Γ -type LPM is lower than that of cascaded T-type LPM with the same cascaded number. Therefore, cascaded Γ -type LPM requires more cascaded numbers to satisfy accuracy demand. The input impedance Z_{in_o} of the single segment is

$$Z_{in_o} = \left(1 - \omega^2 \frac{l}{m} L_0 \frac{l}{m} C_0\right) \left/ \left(j\omega \frac{l}{m} C_0\right) \right. = 1/Z_{in_s} \quad (17)$$

The corresponding series resonance frequency f_s and parallel resonance frequency f_p are both

$$f_s = f_p = \frac{m}{2\pi l \sqrt{L_0 C_0}} \quad (18)$$

Equations (16) and (18) show that the parallel resonance frequency of a single-segment T-type LPM is greater than that of a Γ -type LPM. The ratio is $\sqrt{2}$. This is consistent with the difference in analog accuracy.

3. Determination of Cascaded Number

3.1 Characteristic Impedance of LPM

Characteristic impedance is an inherent characteristic in a transmission line that affects the amplitude and phase changes of voltage and current, equal to the ratio of voltage to current at various locations. The characteristic impedance of the LPM also characterizes the analog accuracy. According to the transmission line theory, the parameters of the accurate equivalent line are expressed as

$$\begin{cases} Z_S = Z_c \sinh(\gamma l) \\ Y_P = \frac{1}{Z_c} \tanh(\gamma l) \end{cases} \quad (19)$$

The distributed parameter model in Fig. 1 can be equivalent through the π -type LPM with the same topology. The equivalent series impedance Z_{pi} and parallel capacitance Y_{pi} of the LPM are expressed as

$$\begin{cases} Z_{pi} = \frac{j\omega L_0 l}{m} \\ Y_{pi} = \frac{j\omega C_0 l}{2m} \end{cases} \quad (20)$$

Compared with (19) and (20), it can be concluded that

$$\begin{cases} Z_{c\pi} = \frac{j\omega L_0 l}{m} \left/ \sinh\left(j\omega \sqrt{L_0 C_0} \frac{l}{m}\right) \right. \\ Z_{c\pi} = \tanh\left(j\omega \sqrt{L_0 C_0} \frac{l}{m}\right) \left/ \frac{j\omega C_0 l}{2m} \right. \end{cases} \quad (21)$$

where $Z_{c\pi}$ is the characteristic impedance of the π -type LPM. Solving (21) yields

$$\sin(\omega l \sqrt{L_0 C_0} / (2m)) = \omega l \sqrt{L_0 C_0} / (2m) \quad (22)$$

Therefore, $Z_{c\pi}$ is

$$Z_{c\pi} = \sqrt{\frac{L_0}{C_0}} \frac{1}{\sqrt{1 - \frac{\pi^2 f^2 l^2 L_0 C_0}{m^2}}} = Z_c k_{pi} \quad (23)$$

The k_{pi} is the characteristic impedance coefficient, which is the ratio of the characteristic impedance of the cascaded π -type LPM to that of DPM. The closer k_{pi} is to 1, the better the equivalence effect of the cascaded π -type LPM is. For the circuit with a fixed cascaded number, the low frequency has higher equivalent accuracy. The accuracy decreases as frequency increases. If high equivalent accuracy is required at the high-frequency band, it is necessary to increase the cascaded number. At 50 Hz, the k_{pi} of the single-cascade circuit is 1.005. This is very high accuracy. Therefore, to investigate the transmission characteristics of the line at the operating frequency, a single-cascade π -type LPM can be selected. It is simple and low-cost. For the frequency of 1000 Hz, the characteristic impedance coefficient is less than 1.01 when the cascaded number is larger than 18. Figure 8 (a) shows k_{pi} with different cascaded numbers and frequencies.

Similarly, the characteristic impedance of cascaded T-type LPM can be also obtained, and is expressed as

$$Z_{cT} = \sqrt{\frac{L_0}{C_0}} \sqrt{1 - \frac{\pi^2 f^2 l^2 L_0 C_0}{m^2}} = Z_c k_T \quad (24)$$

The k_T is the characteristic impedance coefficient of the cascaded T-type LPM. According to (23) and (24), the characteristic impedance of DPM can be expressed as

$$Z_c = \frac{Z_{c\pi}}{k_{pi}} = Z_{cT} k_{pi} \quad (25)$$

Equations (23) and (24) indicate that the characteristic impedance coefficient of cascaded T-type LPM is the reciprocal of that of cascaded π -type LPM. With the increase of cascaded number, their characteristic impedance coefficients are gradually close to 1. Equation (25) shows that although the characteristic impedances of LPMs are different, the ratios to characteristic impedance of DPM are the same. Therefore, the cascaded π -type LPM has the same accuracy with the cascaded T-type LPM.

As shown in Fig. 8, when the cascaded number is 1 and $f > 500$, both k_{pi} and k_T are imaginary numbers. The

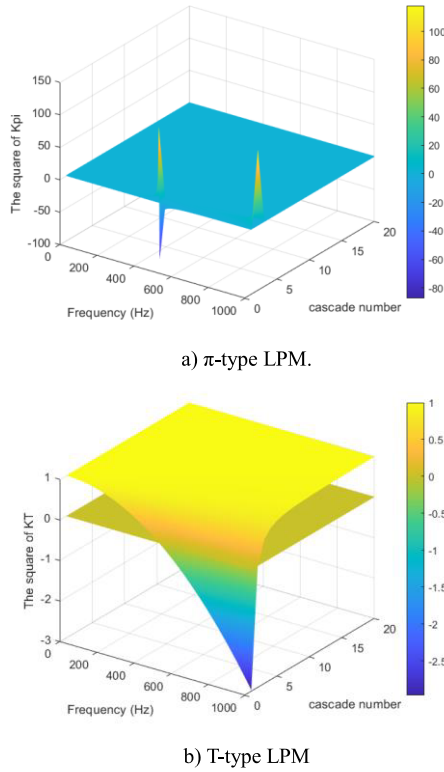


Fig. 8 Characteristic impedance coefficient of LPMs.

LPMs cannot be used for simulation because the characteristic impedance of lossless lines is a positive real number. Therefore, the characteristic impedance of the cascaded LPM should also be a positive real number. For this reason, the cascaded number should satisfy

$$m > \pi f l \sqrt{L_0 C_0} \quad (26)$$

3.2 Cascaded Number

The modal information shows that the same first resonance frequency determines the same cascaded numbers of LPMs. Take the cascaded π -type circuit as an example. According to (23), when k_{pi} is larger than 1, a specific frequency f can be expressed as

$$f = \frac{m \sqrt{k_{pi}^2 - 1}}{\pi l k_{pi} \sqrt{L_0 C_0}} \quad (27)$$

The ratio k_0 of frequency f to the last resonance frequency is expressed as

$$k_0 = \frac{m \sqrt{k_{pi}^2 - 1}}{\pi l k_{pi} \sqrt{L_0 C_0}} \bigg/ \frac{m}{\pi l \sqrt{L_0 C_0}} = \frac{\sqrt{k_{pi}^2 - 1}}{k_{pi}} \quad (28)$$

To improve analog accuracy, the maximum simulation frequency of the cascaded π -type LPM should be less than the first resonance frequency of a single segment. As can

be seen from (14), the ratio of the first resonance frequency to the final resonance frequency is $\sqrt{2}/2$. Therefore, the k_0 of cascaded π -type LPM is less than $\sqrt{2}/2$. So do cascaded T-type LPM. The first resonance frequency of Γ -type LPM is $\sqrt{2}/2$ of the T-type equivalent circuit. The corresponding maximum k_0 is 1/2. Therefore, the k_{pi} of the cascaded Γ -type LPM should be less than $2\sqrt{3}/3$. The optimal cascaded numbers of cascaded π -type, T-type and Γ -type LPMs are shown in (29).

Where f_{max} is the maximum simulation frequency. The $\lceil x \rceil$ is the upward rounding function of x . When the simulation effect demand is not high, k_{pi} can be set to the

$$m_{op} = \begin{cases} \left\lceil k_{pi} \pi f_{max} l \sqrt{\frac{L_0 C_0}{k_{pi}^2 - 1}} \right\rceil & \pi \text{ (T)-type} \\ \left\lceil \sqrt{\frac{3}{2}} k_{pi} \pi f_{max} l \sqrt{\frac{3 L_0 C_0}{2(k_{pi}^2 - 1)}} \right\rceil & \\ = \frac{3}{2} k_{pi} \pi f_{max} l \sqrt{\frac{L_0 C_0}{k_{pi}^2 - 1}} & \Gamma\text{-type} \end{cases} \quad (29)$$

upper limit. When there is a high demand for simulation accuracy, the k_{pi} of the π -type LPM should be reduced. The accuracy of Γ -type LPM decreases in the same proportion.

For the transmission line in Table 1, the wavelength of 3000 Hz is 15.775 km. If the cascaded number is determined based on “1/30 of the wavelength”, a 57-segment LPMs is required. This is a fairly large number. Substituting $m = 57$ to (23) gives

$$k_{pi} = \frac{1}{\sqrt{1 - \frac{\pi^2}{30^2}}} = 1.0055 \quad (30)$$

Equation (30) indicates that the conventional model has a high simulation accuracy. However, for physical simulation systems of general distribution networks, such high simulation accuracy is not necessary. According to (23), when $k_{pi} = \sqrt{2}$, the cascaded number of $m = 9$. Set the k_{pi} between the conventional cascaded number and $\sqrt{2}$, such as $k_{pi} = 1.05$, and the corresponding cascaded number is $m = 20$. The variation curve of m with frequency for different stages is shown in Fig. 9.

It can be seen that when $m = 9$, the change of k_{pi} is significant within 3000 Hz. When $m = 20$ or $m = 57$, k_{pi} remains relatively close to 1. The cascaded number determined by the conventional method is excessive. For distribution network simulation systems with general accuracy requirements, the cascaded number can be determined based on the upper limit of $k_{pi} = \sqrt{2}$.

4. Simulation Verification

According to (29), when $k_{pi} = \sqrt{2}$, the cascaded number of π -type, T-type, and Γ -type LPMs are 8.4, 8.4, and 12.7, respectively. The rounded values are 9, 9 and 13, respectively.

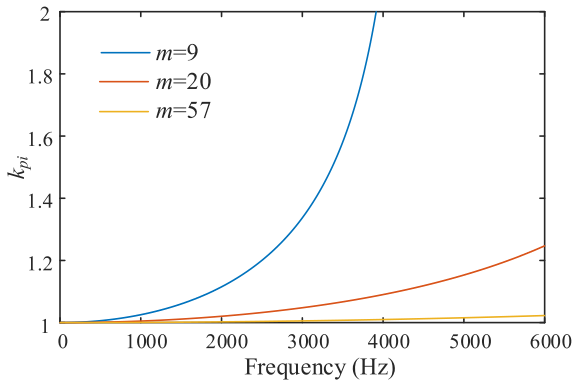


Fig. 9 Characteristic impedance coefficients with different cascaded numbers.

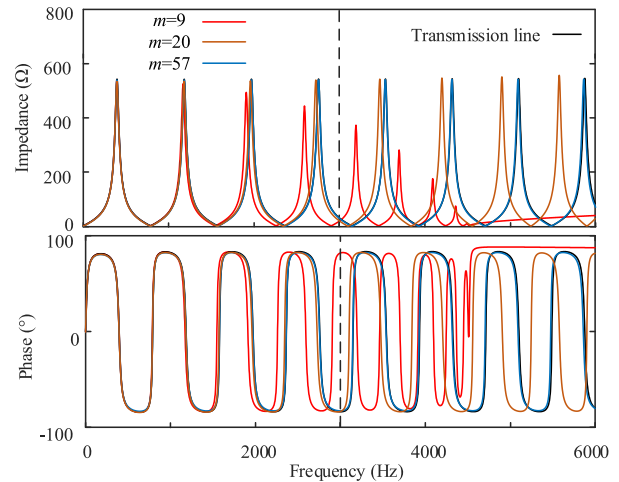


Fig. 11 Frequency characteristics of transmission lines.

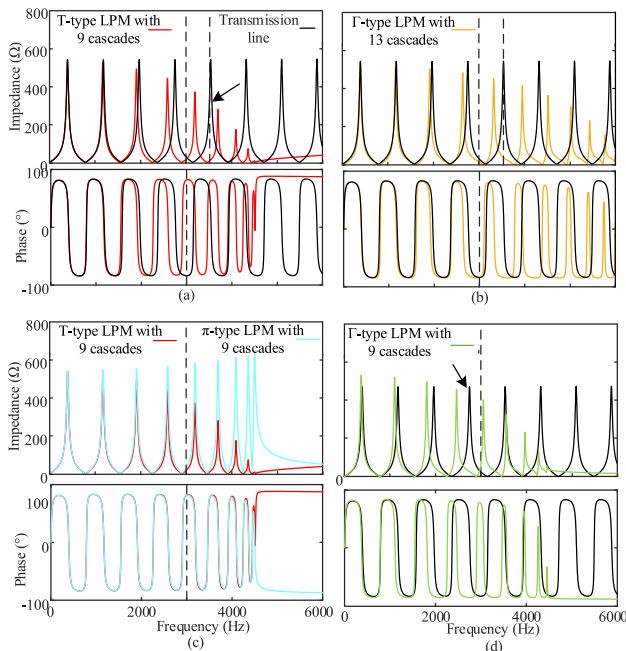


Fig. 10 The results of impedance-frequency scanning.

The line voltage is set to 5.77 kV. The topology of selected cascaded Γ -type LPM is shown in Fig. 6 (a). A 200 V step voltage disturbance is added at the head of the line at 1 s. A resistor of 10Ω of is connected at the end.

Perform impedance-frequency scanning at the end of the line, as shown in Fig. 10. Figure 10 shows that the resonance period of DPM is fixed, while the resonance periods of LPMs gradually decrease. This is consistent with the analysis results based on RMA. From (a) and (b), it can be seen that within 3000 Hz, the impedance characteristics of cascaded π -type, T-type, and Γ -type LPMs are close to that of DPM. When the resonance frequency is greater than 3000 Hz, the difference in resonance characteristics gradually becomes apparent. For example, the $f = 3551$ Hz is the parallel resonance frequency of the DPM. However, it is close to the series resonance frequencies of π (T)-type LPM with 9 cascades and Γ -type LPMs with 13 cascades. Figure 10(c) shows that the π -type and T-type

LPMs have the same impedance characteristics. They have same parallel and series resonance frequencies. Even when $f > 3000$ Hz, the phases of impedance of them are same. When $f > 3000$ Hz, the impedances of π -type and T-type LPMs are remain inductive and capacitive, respectively. As shown in Fig. 10 (d), the Γ -type LPM with 9 cascades have lower accuracy. The $f = 2761$ Hz is the parallel resonance frequency of DPM. But it is close to the series resonance frequencies of Γ -type LPM with 9 cascades. This opposite phenomenon also occurs at $f = 3000$ Hz.

For the cascaded π -type model, Fig. 11 shows the simulation results with different m . Figure 11 shows that as m increases, the cascaded model gradually becomes similar to the transmission line. Within 3000 Hz, the result calculated based on $k_{pi} = \sqrt{2}$, i.e. $m = 9$, also has a good simulation effect. There is no significant difference between the driving point impedances of $m = 20$ and $m = 57$ and the driving point impedance of the transmission line. These four models exhibit four parallel resonances within 3 kHz. When the frequency exceeds 3000 Hz, the model with $m = 9$ deviates significantly from the transmission line. The model with $m = 20$ shows significant differences from the transmission line, and the model with $m = 57$ is still consistent with the transmission line. Therefore, the proposed method meets the simulation requirements of impedance characteristics while reducing costs.

To understand the current response more clearly, the end of the line is connected with a resistance of 1000Ω . The current wave at the headline is shown in Fig. 12. It can be seen that three lumped models have accurate simulation effects. Perform fast Fourier transform (FFT) for one cycle after 1 s. As can be seen from Fig. 13, within a range of less than 3000 Hz, the harmonic content of the distributed parameter model and LPMs are close. DPM and LPMs have significant voltage distortion at 8, 23, 37 and 49 pu. For 49 pu, the harmonic voltage of π -, T-, Γ -type LPMs and DPM are 12.7, 11.5, 11.2 and 11 V, respectively. In frequency band above 3000 Hz, the difference gradually becomes obvious, as shown in Fig. 13. DPM has obvious voltage distortion at

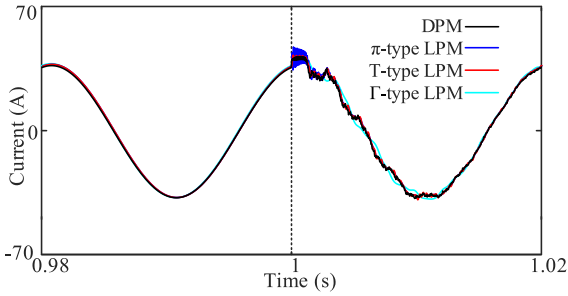


Fig. 12 The head current of distributed parameter model and LPMs.

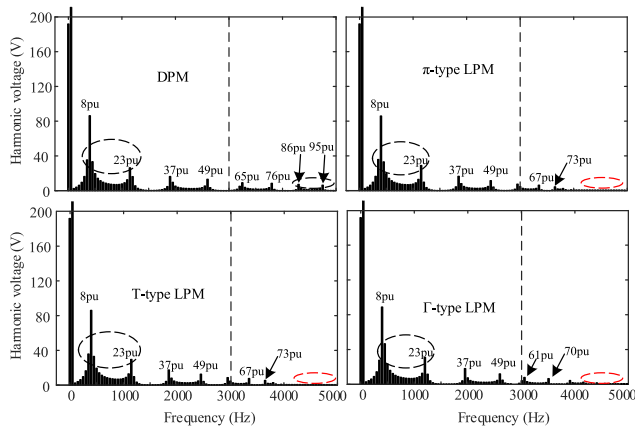


Fig. 13 FFT results of the voltage at the end of line.

65, 76, 86, and 95 pu. However, π -, and T-type LPMs have obvious voltage distortion at 67 and 73 pu. For Γ -type LPM, the resonance frequencies are 61 and 70 pu.

5. Conclusions

This paper proposes a determination method of the cascaded number of the transmission line. The conclusions obtained through theoretical and simulation analysis are as follows.

1) The resonance characteristics of DPM and LPMs are discussed based on RMA and numerical analysis. The resonance frequency and input impedance of transmission lines are periodic. The resonance frequencies of the cascaded π -type and T-type LPMs are equal to the cascaded number, and each resonance frequency is smaller than that of DPM. The number of the resonance frequency of open-circuit Γ -type LPM is equal to the cascaded number minus 1. The number of resonance frequencies of short-circuit Γ -type LPM is equal to the cascaded number. The first resonance frequency characterizes the accuracy of the cascaded LPM.

2) The characteristic impedance coefficients of cascaded π -type LPM and T-type LPM are reciprocal to each other. The LPMs with the same cascaded number of T-type and π -type LPMs have the same accuracy. The accuracy of Γ -type LPM is smaller than that of π -type LPM and T-type LPM with the same cascaded number. The cascaded number for LPMs based on the first resonance frequency of single segment is obtained.

Acknowledgments

This work was supported by the National Key R&D Program: 2019YFE0118000.

References

- [1] P. Dan-Klang and E. Leelarasmee, "Transient simulation of voltage and current distributions within transmission lines," *IEICE Trans. Electron.*, vol.E92-C, no.4, pp.522–531, April 2009.
- [2] H. Cui, F. Li, and K. Tomovic, "Cyber-physical system testbed for power system monitoring and wide-area control verification," *IET Energy Syst. Integr.*, vol.2, no.1, pp.32–39, 2020.
- [3] B. Hou, Y. Zhang, Y. Guo, Q. Guo, B. Xi, and H. Sun, "Information flow based cyber-physical power system modeling and simulation," 2021 IEEE 5th Conference on Energy Internet and Energy System Integration (EI2), Taiyuan, China, pp.326–330, 2021.
- [4] J. Kim, E. Song, J. Cho, Y. Shim, G. Kim, and J. Kim, "Frequency-dependent transmission line model of a stranded coaxial cable," *IEICE Trans. Electron.*, vol.E93-C, no.1, pp.112–119, Jan. 2010.
- [5] L. Hu, W. Lei, J. Zhao, and X. Sun, "Optimal weighting factor design of finite control set model predictive control based on multiobjective ant colony optimization," *IEEE Trans. Ind. Electron.*, Early Access, 2023.
- [6] W. Pan, Y. Li, and X. Chen, "Calculation method of corona loss in EHV/UHV system based on distributed parameter characteristic," *IEEJ Trans. Electr. Electron. Eng.*, vol.14, no.5, pp.730–734, 2019.
- [7] A.R. Al-Roomi and M.E. El-Hawary, "A novel approach to precisely calculate lumped parameters for transmission lines with sag using the M-model equivalent circuit," 2020 IEEE Electric Power and Energy Conference (EPEC), Edmonton, AB, Canada, pp.1–6, 2020.
- [8] H. Peng, W. Mo, Y. Wang, L. Luan, and Z. Xu, "Fault location algorithm for multi-terminal transmission lines of distribution system based on loop-analysis," 2021 IEEE 5th Conference on Energy Internet and Energy System Integration (EI2), Taiyuan, China, pp.1094–1100, 2021.
- [9] K. Wada, H. Fujita and H. Akagi, "Considerations of a shunt active filter based on voltage detection for installation on a long distribution feeder," *IEEE Trans. Ind. Appl.*, vol.38, no.4, pp.1123–1130, July-Aug. 2002.
- [10] D. Oliveira, G.C.B. Leal, D. Herrera, E. Galván-Díez, J.M. Carrasco, and M. Aredes, "An analysis on the VSC-HVDC contribution for the static voltage stability margin and effective short circuit ratio enhancement in hybrid multi-infeed HVDC Systems," *Energies*, vol.16, no.1, 532, 2023.
- [11] Z. Liu, H. Gao, and S. Luo, "Non-unit protection for long-distance LCC-HVDC transmission lines based on waveform characteristics of voltage travelling waves," *Int. J. Electr. Power Energy Syst.*, vol.150, 109079, 2023.
- [12] R. Dias, A. Lima, C. Portela, and M. Aredes, "Extra long-distance bulk power transmission," *IEEE Trans. Power Deliv.*, vol.26, no.3, pp.1440–1448, July 2011.
- [13] E.C. Gomes and M.C. Tavares, "Analysis of the energization test of a half-wavelength AC link composed of similar transmission lines," 2011 Asia-Pacific Power and Energy Engineering Conference, Wuhan, China, 2011.
- [14] W. Lin, J. Yi, F. Yu, J. Jia, A. Wang, and X. Wang, "Analysis of half-wavelength transmission lines system state in operation," 2019 IEEE Innovative Smart Grid Technologies - Asia (ISGT Asia), Chengdu, China, pp.741–746, 2019.
- [15] Q. Yu and O. Wing, "Computational models of transmission lines with skin effects and dielectric loss," *IEEE Trans. Circuits Syst. I: Fundam. Theor. Appl.*, vol.41, no.2, pp.107–119, Feb. 1994.
- [16] X. Li, Z. Xu, Q. Lai, and Z. Zhang, "Research on transmission line model based on phase-mode transformation in HVDC system," *IEEJ*

- Trans. Electr. Electron. Eng., vol.15, no.1, pp.51–60, 2020.
- [17] E. Leelarasmee and P. Naenna, "A distributed state variables approach to the transmission lines transient simulation," The 2004 IEEE Asia-Pacific Conference on Circuits and Systems, Tainan, Taiwan, vol.1, pp.73–76, 2004.
- [18] M.S. Mamis, "Discrete-time state-space modeling of distributed parameter transmission line," EUROCON 2007 - The International Conference on "Computer as a Tool", Warsaw, Poland, pp.2078–2081, 2007.
- [19] X. Zhou, X. Lu, W. Wang, J. Ren, and Y. Gu, "Establishment of transmission lines model of shielded twisted-pair line," IEICE Trans. Electron., vol.E106-C, no.3, pp.67–75, March 2023.
- [20] A. Ramirez, A. Semlyen, and R. Iravani, "Harmonic domain characterization of the resonant interaction between generator and transmission line," IEEE Trans. Power Deliv., vol.20, no.2, pp.1753–1762, April 2005.
- [21] J.R. Harries and J.L. Randall, "Harmonic resonance on parallel high voltage transmission lines," IEEE Trans. Power Deliv., vol.12, no.1, pp.477–482, Jan. 1997.
- [22] J.W. Phinney, D.J. Perreault, and J.H. Lang, "Synthesis of lumped transmission-line analogs," IEEE Trans. Power Electron., vol.22, no.4, pp.1531–1542, July 2007.
- [23] S. Kurokawa, F.N.R. Yamanaka, A.J. Prado, and J. Pissolato, "Inclusion of the frequency effect in the lumped parameters transmission line model: State space formulation," Electr. Power Syst. Res., vol.79, no.7, pp.1155–1163, 2009.
- [24] O.I. Elgerd, Electric energy systems theory, McGraw-Hill, New York, 1982.
- [25] X. Cui, "Chained number of lumped-circuits for physical analogy of the lossless transmission lines," Proc. CSEE, vol.9, pp.2561–2571, 2017.
- [26] R. Zhan, Y. Li, Y. Yu, J. Meng, and B. Wang, "The number of chained lumped-circuits for the physical analogy of half-wavelength power transmission lines," 2017 IEEE 5th International Symposium on Electromagnetic Compatibility (EMC-Beijing), Beijing, China, pp.1–5, 2017.
- [27] Y. Li, C. Jiao, and B. Wang, "The number of chained π -type circuits for dynamic analogy of half-wavelength transmission line considering short-circuit fault," 2017 Sixth Asia-Pacific Conference on Antennas and Propagation (APCAP), Xi'an, China, pp.1–3, 2017.
- [28] W. Xu, Z. Huang, Y. Cui, and H. Wang, "Harmonic resonance mode analysis," IEEE Trans. Power Deliv., vol.20, no.2, pp.1182–1190, April 2005.
- [29] Z. Huang, Y. Cui, and W. Xu, "Application of modal sensitivity for power system harmonic resonance analysis," IEEE Trans. Power Syst., vol.22, no.1, pp.222–231, Feb. 2007.
- [30] K.S. Oh, "Accurate transient simulation of transmission lines with the skin effect," IEEE Trans. Comput.-Aided Des. Integr. Circuits Syst., vol.19, no.3, pp.389–396, March 2000.
- [31] J.E. Schutt-Aine, "High-frequency characterization of twisted-pair cables," IEEE Trans. Commun., vol.49, no.4, pp.598–601, April 2001.



Risheng Qin graduated from Guangxi University, Nanning, China, majoring in Power System and Automation. He was employed by Electric Power Science Research Institute of Yunnan Power Grid Co. Ltd. His research interests include power quality management and model predictive control.



Hua Kuang graduated from Kunming University of Science and Technology, Kunming, China, majoring in Power System and Automation. He was employed by Production Technology Department of Yunnan Power Grid Co. Ltd. His research interests include voltage and reactive power management, and control of power converters.



He Jiang graduated from North China Electric Power University, Beijing, China, majoring in Power Systems and Automation. He was employed by Electric Power Science Research Institute of Yunnan Power Grid Co. Ltd. His research interests include power quality management and multilevel converters.



Hui Yu graduated from Taiyuan University of Technology, Taiyuan, China, majoring in Power Systems and Automation. He was employed by Electric Power Science Research Institute of Yunnan Power Grid Co. Ltd. His research interests include power system analysis and grid-tied power converters.



Hong Li graduated from Honghe University, Honghe, China, majoring in Electrical Engineering and Its Automation. She was employed by Honghe Power Supply Bureau of Yunnan Power Grid Co. Ltd. Her research interests include the control strategy of reactive power and voltage in the distribution network.



Zhuan Li graduated from Wuhan University, Wuhan, China, majoring in Power System and Its Automation. He was employed by Dali Power Supply Bureau of Yunnan Power Grid Co. Ltd. His research interests include power quality management and grid-tied power converters.